Combustion and Flame 159 (2012) 194–199

Contents lists available at ScienceDirect

Combustion and Flame

journal homepage: www.elsevier.com/locate/combustflame

Numerical investigation of spherical diffusion flames at their sooting limits

V.R. Lecoustre [a], P.B. Sunderland [a,*], B.H. Chao [b], R.L. Axelbaum [c]

[a] Department of Fire Protection Engineering, University of Maryland, College Park, MD 20742, USA
[b] Department of Mechanical Engineering, University of Hawaii, Honolulu, HI 96822, USA
[c] Department of Energy, Environmental and Chemical Engineering, Washington University in St. Louis, St. Louis, MO 63130, USA

ARTICLE INFO

Article history:
Received 17 December 2010
Received in revised form 26 May 2011
Accepted 27 May 2011
Available online 29 June 2011

Keywords:
Laminar flames
Microgravity
Soot

ABSTRACT

Detailed numerical simulations are presented of laminar microgravity spherical diffusion flames at their experimentally observed sooting limits. Ten normal and inverse flames fueled by ethylene are considered. Observed in a drop tower, these flames were initially sooty but reached their sooting limits 2 s after ignition (or slightly before). The flames span broad ranges of stoichiometric mixture fraction (0.065–0.692), adiabatic flame temperature (2226–2670 K), and stoichiometric scalar dissipation rate (0.013–0.384 s^{-1}). They were modeled using a one-dimensional, transient diffusion flame code with detailed chemistry (up to toluene) and transport. Radiative losses from products were modeled using a detailed absorption/emission statistical narrow-band model coupled with a discrete-ordinates method. Flame structure at the sooting limits was examined, emphasizing the behavior of carbon to oxygen atom ratio, temperature, and scalar dissipation rate. For ethylene flames with sufficiently long flow times it was found that soot formation coincides with regions where the C/O atom ratio and temperature exceed critical values, specifically 0.53 and 1305 K, respectively. The scatter about these critical values is small, which is noteworthy considering the wide range of flame conditions. These observations are consistent with the expected effects of H radicals on the propargyl soot pathway.

1. Introduction

Sooting limits are the conditions associated with incipient soot formation and are fundamental measures of the sooting propensity of fuels. Sooting limits in premixed flames are understood to arise when the rates of fuel pyrolysis and soot precursor oxidation are equal [1]. There have been extensive measurements of sooting limits in laminar premixed flames [1–7]. These limits normally are expressed in terms of the carbon-to-oxygen atom ratio, C/O, for a given fuel. For example, in premixed ethylene flames, C/O_c (where the subscript denotes conditions critical for soot formation) is between 0.55 and 0.6 [1,3–5,7]. For most fuels, C/O_c does not vary with temperature (i.e., amount of inert) [4].

It has been observed that the *local* C/O (along with a critical local temperature, T_c) is also an important parameter for identifying sooting limits in non-premixed flames [8–11]. Specifically, considering the location in the flame where C/O equals C/O_c, the flame reaches a sooting limit when the temperature at that location reaches a critical temperature. Tests of spherical microgravity ethylene diffusion flames [9] estimated C/O_c and T_c through a Burke–Schumann based analysis to be 0.59 and 1838 K, while tests of coflow diffusion flames in normal gravity [10,11] found C/O_c between 0.53 and 0.6 and local critical temperature, T_c, between 1627 and 1640 K. These values for C/O_c are close to those observed in ethylene premixed flames. Early work [8–11] suggested that this may be due to competition between fuel pyrolysis and soot precursor oxidation similar to that which occurs in premixed flames. More recent modeling in diffusion flames, however, shows that C/O_c indicates the edge of the region containing H radicals, which consume the key soot precursor C_3H_3 [12].

While temperature has little effect on premixed flame sooting limits, it is critical in diffusion flame sooting limits. Experimental diffusion flame studies have identified a critical local temperature for soot formation of 1250–1650 K [5,11,13–16]. Diffusion flames with *peak* temperatures much higher than T_c will nevertheless be soot free if the *local* temperature is below T_c everywhere that the local composition (indicated by C/O) is otherwise suitable for soot formation.

Soot formation kinetics are relatively slow, thus requiring sufficiently long flow time. Soot induction times of 0.8–15 ms were reported by Tesner and Shurupov [17] for acetylene/nitrogen mixtures at 1473 K. A soot carbonization time of 1.8–11.9 ms was predicted by Dobbins [16]. Strain rates above 30–200 s^{-1} (depending on the amount of fuel dilution) were observed to prevent soot formation in counterflow ethylene diffusion flames [18–20]. Flow times that are extremely long, as can be obtained in microgravity flames, can inhibit soot formation via radiative losses.

* Corresponding author. Fax: +1 301 405 9383.
E-mail address: pbs@umd.edu (P.B. Sunderland).

0010-2180/$ - see front matter © 2011 The Combustion Institute. Published by Elsevier Inc. All rights reserved.
doi:10.1016/j.combustflame.2011.05.022

Although strain-free flames can be obtained in microgravity spherical flames, potentially yielding new insights into sooting limits, their large radiative losses can complicate interpretation of the data [21].

Recognizing the importance of local C/O, T, and flow time for soot formation in diffusion flames, past work has hypothesized that soot formation in diffusion flames requires a region where C/O, T, and flow time are above their critical values [9,11]. An equivalent statement of this hypothesis is that sooting limits arise when C/O and T reach their critical values at the same location (except for flames with extremely short flow times, which require a higher local temperature for soot inception). Sunderland et al. [9] proposed this hypothesis, and found it to be supported by a simple analysis of sooting limits of spherical diffusion flames. Kumfer et al. [11], considering sooting limits of coflow ethylene diffusion flames, further supported the hypothesis and extended the theory to include residence time effects. Both studies found the soot formation region to be bounded on its rich side by temperatures below T_c and on its lean side by C/O below C/O_c. Further work is warranted, however, as Ref. [9] invoked a very simple model of local T and C/O, and Ref. [11] was limited by the conditions available in normal gravity.

Spherical microgravity diffusion flames are attractive for studying sooting limits of diffusion flames for several reasons. They can be simulated using a one-dimensional numerical model. They avoid the intrusion of strain that is inherent in counterflow diffusion flame studies, and allow the observation of flames with a very broad range of flow times. They avoid the complicated streamlines of coflow diffusion flames, allowing observations of both normal and inverse diffusion flames.

Thus motivated, the objectives of this work are to numerically investigate the sooting limits of the microgravity spherical diffusion flames of [9], and to evaluate the hypothesis that these limits are associated with conditions where C/O and T reach their critical values at the same location (except for flames with extremely short flow times). Owing to the wide range of conditions of these flames, they offer a robust test of the hypothesis.

2. Experimental methods

The flames considered here were studied in microgravity using the NASA Glenn 2.2 s drop tower and were initially reported in Sunderland et al. [9]. The burner was a 6.4 mm diameter porous stainless steel sphere. All tests were conducted in a quiescent ambient at 295 K and 0.98 bar. Ignition was performed immediately after release into microgravity. The tests employed three gases: ethylene, nitrogen, and oxygen. A color video camera was used to image the flames. Experimental details are in [9,21,22].

A summary of the 17 sooting limit flames of [9] is given in Table 1. (These will be downselected below to 10 flames.) A large number of experiments were conducted to identify these sooting limit flames, which initially contained yellow regions, but became blue at 2 s after ignition (or slightly before). Burner flow rates were selected such that all flames involved a steady-state ethylene consumption rate of 1.51 mg/s, generating 71 W for complete combustion. Experiments were conducted with *normal* and *inverse* flames corresponding to ambients containing oxidizer or fuel, respectively. The fuel and oxygen mole fractions in the supply gases, $X_{C2H4,f}$ and $X_{O2,ox}$, were varied as widely as possible. Adiabatic flame temperatures, T_{ad}, were calculated using CEA [23] and are shown in Table 1.

3. Numerical methods

The flames were simulated using a one-dimensional diffusion flame solver modified from Sandia's PREMIX code [24]. Similar simulations are reported in [21,25,26]. The solver was combined with Sandia's CHEMKIN and Transport packages [27,28] to handle detailed chemistry and transport. Although Santa et al. [25] augmented species and heat diffusivities by 30%, no such augmentation was used here. Viscosity was neglected and constant pressure ideal gas behavior was assumed.

Conservation equations for mass, species, and energy were solved. The conservation equations were discretized on a non-uniform mesh using a central difference operator for the diffusive terms. The convective terms were discretized using either a first-order backward difference operator (for continuity) or a second-order central difference operator (for the energy and species conservation equations). Implicit first-order time marching was used. The equations were solved using Sandia's Twopnt [29], which uses a modified damped Newton's method to solve boundary value problems.

The inner boundary of the computational domain was the spherical burner surface, where the imposed conditions were a steady species mass flux and either an adiabatic boundary (for steady state computations) or a temperature of 300 K (for transient calculations). At the outer boundary a temperature of 300 K was specified. Pressure was held constant at 0.98 bar.

Emission and reabsorption of radiation were included, considering the participation of CO_2, H_2O, and CO. Radiative heat losses

Table 1
Summary of the 17 experimentally identified sooting limit flames at 2 s.[a]

Flame	Environment	$X_{C2H4,f}$	$X_{O2,ox}$	Z_{st}	T_{ad} (K)	χ_{st} (s^{-1})	r^*	d_{meas} (mm)	d_{pred}/d_{meas}
1	Oxidizer	1	0.22	0.065	2390	0.013	0.06	28.8 ± 2.7	1.09
2	Oxidizer	0.6	0.21	0.102	2326	0.028	0.06	30 ± 1	1.10
3	Oxidizer	0.31	0.21	0.180	2226	0.085	0.10	33 ± 1.7	1.02
4	Oxidizer	0.25	0.23	0.225	2238	0.100	0.09	33.4 ± 2.8	1.00
5	Oxidizer	0.18	0.28	0.333	2306	0.230	0.07	29.9	1.04
6	Oxidizer	0.17	0.29	0.353	2308	0.253	0.06	29.3	1.05
7	Oxidizer	0.11	0.5	0.586	2381	0.609	0.10	22.5	1.14
8	Oxidizer	0.11	0.8	0.685	2528	1.143	0.10	16.4	1.24
9	Oxidizer	0.15	1	0.661	2740	2.149	0.14	11.6	1.37
10	Fuel	1	0.13	0.041	1847	0.052	0.25	17.5	1.42
11	Fuel	0.8	0.13	0.051	1835	0.061	0.17	20.3	1.29
12	Fuel	0.6	0.13	0.066	1814	0.082	0.18	21.8	1.28
13	Fuel	0.21	0.25	0.277	2274	0.269	0.17	29.6	0.97
14	Fuel	0.19	0.3	0.336	2370	0.344	0.08	28.3	0.98
15	Fuel	0.15	0.5	0.509	2539	0.384	0.06	27.5	0.97
16	Fuel	0.12	0.8	0.666	2578	0.240	0.05	25.9	1.08
17	Fuel	0.13	1	0.692	2670	0.244	0.05	25	1.03

[a] Reproduced in part from [9]. Flames 1–6 and 14–17 have acceptable sphericity and agreement between predicted and measured diameters.

were obtained by solving the radiative transfer equation using a discrete-ordinates method [30] with Gaussian–Legendre quadrature over 20 ordinates. The radiative properties were formulated using a statistical narrow-band model with exponential-tailed inverse line strength distributions for wavenumbers of 150–9300 cm^{-1} divided into 366 bands with a 25 cm^{-1} spectral bandwidth [31]. Species radiation parameters were taken from the HITRAN database [32]. Radiative properties were pre-computed and then accessed when needed.

Because this work emphasizes flames at their sooting limits, only gas phase chemistry was modeled. The chemical kinetics model was USC Mech Version II [33]. This is a $H_2/CO/C_1$-C_4 reaction model based on: an optimized reaction model of H_2/CO; GRI-Mech 1.2 and 3.0; and a comprehensive reaction kinetic model of ethylene, acetylene, propene, and 1,3-butadiene oxidation at high temperature. It also includes formation and oxidation of benzene and toluene. The model has been validated with $H_2/CO/C_1$–C_4 flame measurements [33]. Additional reactions were included to model polyaromatic hydrocarbon (PAH) formation from benzene to pyrene [34].

Ignition in the numerical model followed past work whereby a steady-state adiabatic non-radiative solution of each flame was obtained in a compressed domain [21,25,26,35], with its outer boundary 1.2 cm from the origin. The outer boundary was then extended to a radius of 20 cm and the transient simulation commenced.

Non-uniform grids were generated, with finer spacing in regions of high gradients. The transient simulations typically used 200 mesh points. Temperature and species gradients at the outer boundary were found to be negligible for transient cases within 3 s of ignition; for all flames at 3 s the thermal fields extended to less than 8 cm. Thus, the location of the outer boundary had a negligible impact on the results presented here. Radiative heat losses were considered for all transient simulations.

4. Results and discussion

Most of the 17 experimental flames had nearly spherical shapes at 2 s, particularly those with low nitrogen concentrations in the burner gas. Flame sphericity was measured from images of the flames at 2 s, accepting that only one camera view was available. For each flame, the flame radii were measured in eight evenly distributed directions, and for these the standard deviation divided by the mean was found. Values of this quantity, denoted r^*, are reported in Table 1. Owing to the importance of sphericity in sooting limits, flames for which r^* exceeded 0.1, namely flames 9–13, were excluded from the analysis that follows.

The 17 flames in Table 1 were simulated at ignition and for 3 s afterward. For some flames the predicted and measured diameters, d_{pred} and d_{meas}, were not in agreement, as shown in Table 1. This is attributed to experimental and computational inaccuracies, particularly those associated with ignition. The predicted diameters were defined as those at peak temperature. Flames for which d_{pred} was not within ±10% of d_{meas}, namely flames 7–12, were excluded from the analysis that follows. These flames were not accurately represented by the numerical simulations. Following these exclusions, 10 flames remained: flames 1–6 and 14–17.

Experiments and computations indicate that none of the flames reached steady state within 2 s. Microgravity experiments have shown that flame diameters can briefly decrease after ignition, but then increase with time [22,25,26]. These increasing diameters have been captured computationally [21,25,26,35] and lead to reduced peak temperatures because radiative losses are proportional to flame diameter squared [21]. At 2 s, the predicted peak temperatures for the 10 flames varied from 1442 to 2316 K and averaged about 700 K below their adiabatic flame temperatures. The peak temperatures were above the 1100 K temperature identified for radiative extinction of spherical ethylene diffusion flames [21,36]. At 2 s after ignition the radiative heat loss fractions were around 0.55 for all flames except flames 10–12, which had radiative heat loss fractions of about 0.4.

The simplest characteristic time for these flames is the residence time, defined as the time for a fluid parcel to convect from the burner to the location of peak temperature [9]. For inverse flames this definition can be misleading because it pertains to the oxidizer side. Thus, a flow time based only on local conditions is adopted here, namely χ^{-1}, where χ is the local scalar dissipation rate:

$$\chi = 2\alpha(dZ/dr)^2. \tag{1}$$

Here α is local thermal diffusivity, Z is mixture fraction, and r is radius. The scalar dissipation rate at the location of peak temperature, χ_{st}, is reported for the present flames in Table 1. For these flames χ_{st}^{-1} generally increases with increasing residence time.

Stoichiometric mixture fraction for these flames is defined as [8]:

$$Z_{st} = [1 + 3X_{C2H4,f}(0.143 + 1/X_{O2,ox})]^{-1}, \tag{2}$$

where X is mole fraction and subscripts f and ox denote the fuel and oxidizer supplies. Local mixture fraction is normally defined as the local mass fraction of the elements that originated in the fuel supply. This is complicated here by the presence of N_2 in both the fuel and the oxidizer. Thus, an alternative local mixture fraction [37,38] for ethylene combustion is invoked,

$$Z = \frac{\frac{Y_H}{4M_H} + \frac{Y_C}{2M_C} + \frac{Y_{O,ox} - Y_O}{3M_O}}{\frac{Y_{H,f}}{4M_H} + \frac{Y_{C,f}}{2M_C} + \frac{Y_{O,ox}}{3M_O}}, \tag{3}$$

where Y is mass fraction, the capitalized subscripts denote the element considered, and M is element mass.

Distributions of T, C/O, Z, and χ were computed for the 10 flames at 2 s after ignition, which is when the flames were observed to reach their sooting limits. Figure 1 plots these profiles for flame 1 (a typical normal flame) and flame 17 (a typical inverse flame). In both flames, as expected the temperature peaks near where $Z = Z_{st}$ and near where $C/O = 0.333$. The highest scalar dissipation rates are near the burner, and product diffusion to the burner surface is evident from the values of Z there.

The highest C/O occurs at the burner for normal flames and at the ambient boundary for inverse flames. In both cases, as the fuel approaches regions hot enough for soot to form, C/O decreases below values that can support soot formation. It will be shown below that Fig. 1a and b depict conditions where, moving from the fuel source toward the reaction zone, temperature increases above T_c near where C/O falls below C/O_c.

The hypothesis that sooting limits correspond to conditions where both T and C/O reach their critical values at the same location is supported if a single pair of critical values applies for all 10 flames. For flames with very short flow times, the critical temperature for soot formation may increase, but otherwise the competition between C/O and temperature is expected to be only weakly affected by flow time [9,11]. We next investigate this hypothesis.

Figure 2 plots T as a function of local C/O for the 10 flames. The region of potential soot formation is where both C/O and T are high. Figure 2 reveals a region of converging curves near $C/O = 0.53$ and $T = 1305$ K. (The identification of these values is explained below.) This suggests that the hypothesis is supported by these flames.

For each temperature, the associated C/O on the fuel side was found for every flame. For each such temperature, the standard

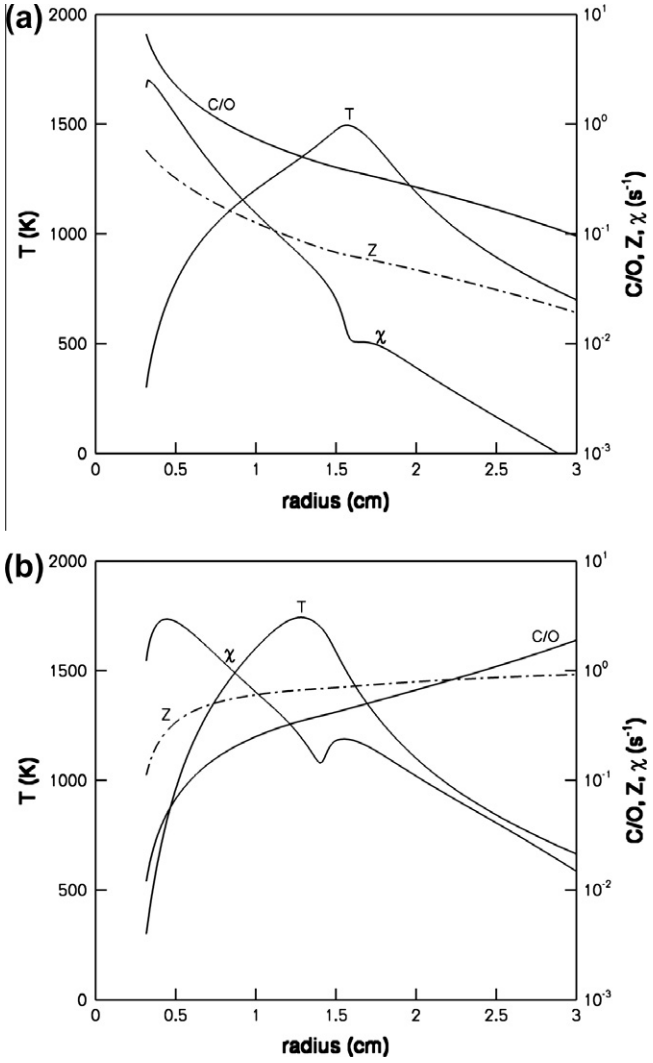

Fig. 1. Predicted T, C/O, Z, and χ profiles at 2 s after ignition for (a) normal flame 1 and (b) inverse flame 17.

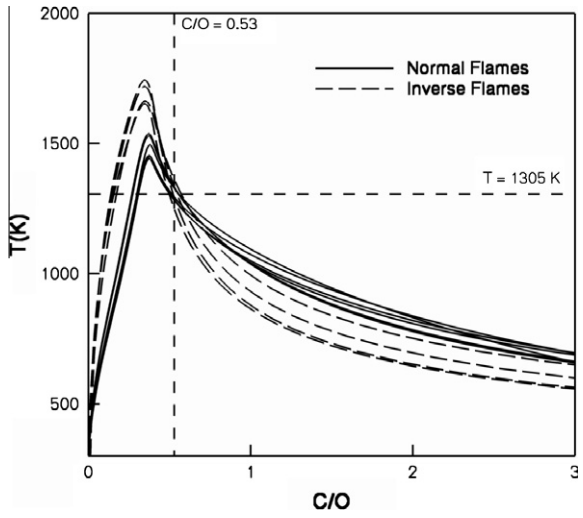

Fig. 2. Predicted T as a function of C/O for flames 1–6 and 14–17.

deviation of these C/O divided by their mean, C/O^*, was obtained and plotted as shown in Fig. 3. The mean C/O also is plotted. Quantity C/O^* has a minimum at $C/O = 0.53$ and $T = 1305$ K. Thus, the

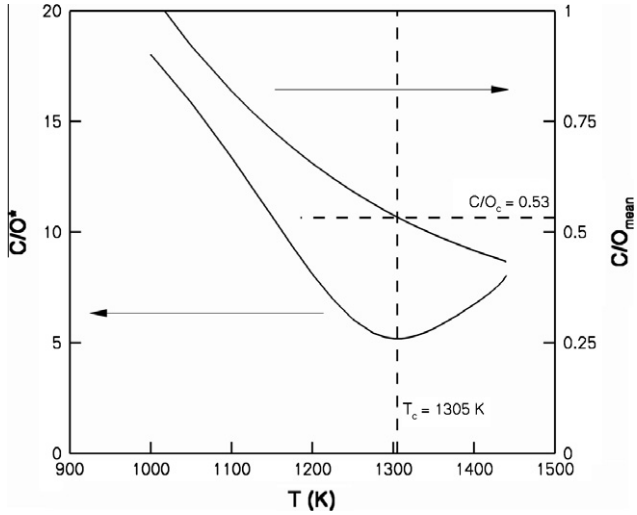

Fig. 3. Predicted C/O^*, percent, and C/O_{mean} plotted with respect to local temperature at 2 s after ignition.

critical conditions for soot formation in these ethylene flames is established as $C/O_c = 0.53$ and $T_c = 1305$ K. This value of C/O_c is close to previous values obtained in ethylene premixed [1,3–5,7] and diffusion flames [9–11], while this value of T_c is close to values obtained in normal gravity [10,11] diffusion flames. When performing the same analysis including all 17 flames, the critical temperature was found to be 1360 K, which corresponds to a critical C/O of 0.55. However, the scatter increases by about a factor of 5.

Having identified C/O_c and T_c, it is possible to evaluate the scatter about these conditions for the 10 flames. For each flame Fig. 4a shows C/O_{1305}, which is C/O on the fuel side where $T = 1305$ K, plotted with respect to inverse scalar dissipation rate at this location, denoted $1/\chi_{0.53}$. The mean C/O_{1305} is 0.53, with reasonably low scatter. For each flame Fig. 4a also plots $T_{0.53}$, defined as the temperature where $C/O = 0.53$. The mean $T_{0.53}$ is 1305 K, again with reasonably low scatter. Quantities C/O_{1305} and $T_{0.53}$ are plotted in Fig. 4b with respect to Z_{st}. It is remarkable to find such uniformity of the critical C/O and T for soot formation for conditions with such wide variations in fuel and oxidizer supply mole fractions, Z_{st}, T_{ad}, scalar dissipation rates, and convection directions.

Further insight into sooting limit phenomena can be obtained from plots of local T and C/O versus Z. Such plots are shown in Fig. 5 for flames 1 and 17, which are the normal and inverse sooting limit flames considered in Fig. 1. These flames have relatively high flow times. For clarity, the y-axes of Fig. 5 are scaled such that $T = 1305$ K aligns with $C/O = 0.53$. Figure 5 shows that, when moving from the fuel supply toward the peak temperature, C/O for both flames falls below its critical value (0.53) at the location where temperature increases above its critical value (1305 K). Similar behavior was observed for the other 8 flames.

Figure 6 considers flame 5, at times of 0.5, 1, and 2 s after ignition, using the same axes as Fig. 5. This allows the flame evolution to be followed temporally. Figure 6 also includes color images of flame 5 recorded at these times, onto which are superimposed the associated contours of predicted peak temperature. At times of 0.5 and 1.0 s, abundant yellow emission from soot is observed. This agrees with the computations, which reveal regions at these early times where both T and C/O are well in excess of 1305 K and 0.53. In contrast, at 2 s the experiments reveal a sooting limit and the computations predict a vanishing region with $T > 1305$ K and $C/O > 0.53$. This plot shows how a complication of drop tower testing – unsteady burning – can be exploited in the study of sooting limits.

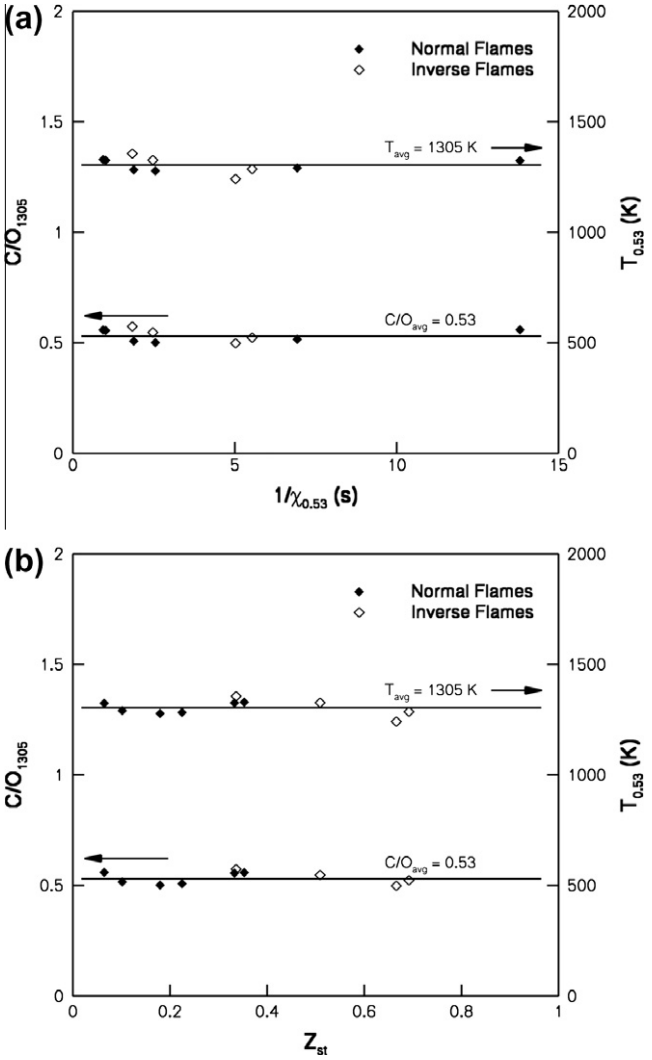

Fig. 4. Predicted C/O at $T = 1305$ K and temperature where $C/O = 0.53$ for the sooting limit flames at 2 s, plotted with respect to (a) inverse scalar dissipation rate where $C/O = 0.53$ and (b) stoichiometric mixture fraction.

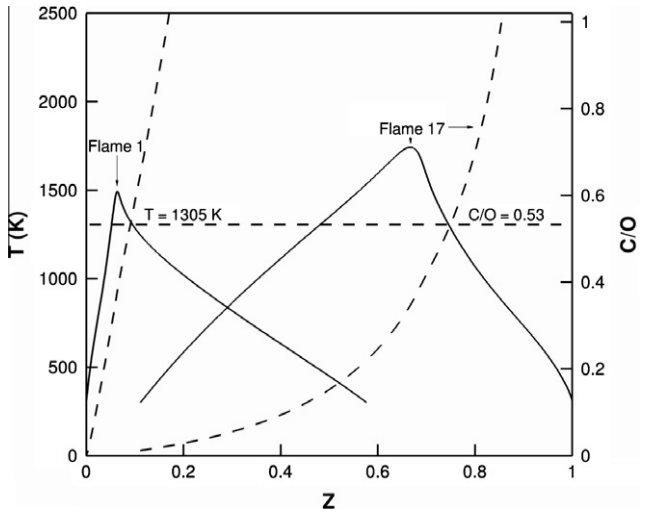

Fig. 5. Temperature (solid curves) and C/O profiles (dashed curves) in Z space for normal flame 1 and inverse flame 17 at 2 s after ignition.

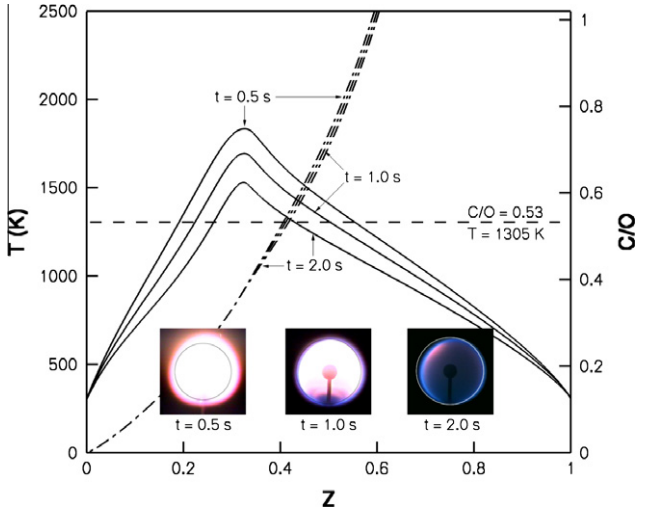

Fig. 6. Temporal evolution of T (solid curves) and C/O (dash-dot curves) in Z space for flame 5. Color images of the flame at 0.5, 1.0, and 2 s are shown with superimposed predicted contours of peak temperature. (For interpretation of the references to color in this figure legend, the reader is referred to the web version of this article.)

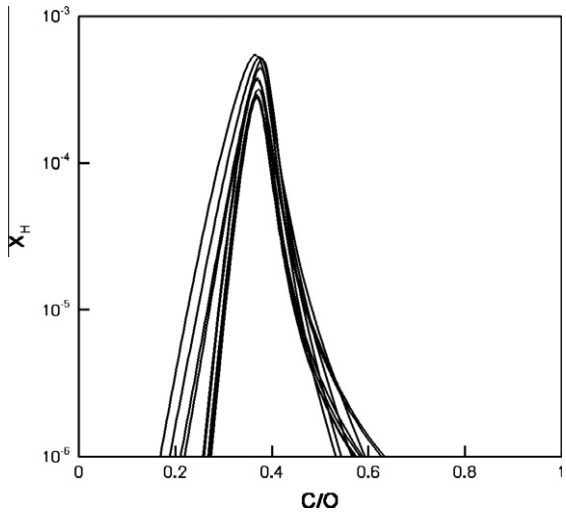

Fig. 7. Predicted mole fraction profiles of H radical with respect to local C/O for the sooting limits flames at 2 s.

H radicals can suppress soot inception by removing propargyl. Propargyl is an important intermediate species in the formation of the first large PAH, through propyne dissociation [34]. For instance, in ethylene flames propargyl is the main precursor of phenyl, which is a key species in forming PAH [34]. H radicals contribute to propargyl removal by $C_3H_3 + H \Rightarrow pC_3H_4$ followed by $pC_3H_4 + H \Rightarrow C_2H_2 + CH_3$. Figure 7 plots the predicted H radical mole fractions with respect to the local C/O for the 10 flames at their experimentally observed sooting limits. These flames have similar H profiles. The critical C/O of 0.53 is roughly coincident with the upper boundary of H radical.

5. Conclusions

This study sought to evaluate, for a very broad range of conditions, the hypothesis that soot formation in diffusion flames requires a region where C/O, temperature, and flow time exceed their critical values. Transient simulations of spherical diffusion

flames at their sooting limits, facilitated by the one-dimensional nature of the flames, were performed using detailed chemistry, transport, and radiation. The major conclusions are as follows.

(1) Numerical predictions of microgravity ethylene spherical diffusion flames support the hypothesis that soot formation in diffusion flames requires a region where C/O, temperature, and flow time exceed their critical values.
(2) The critical values for C/O and temperature for these flames are 1305 K and 0.53 for ethylene, and the scatter about these values is small.
(3) This hypothesis is supported for a very broad range of conditions, many of which cannot be obtained in normal gravity. The present conditions included transient flames, reactant supply mole fractions of 0.12–1, stoichiometric mixture fractions of 0.065–0.692, adiabatic flame temperatures of 2226–2670 K, stoichiometric scalar dissipation rates of 0.013–0.384 s^{-1}, and both normal and inverse convection directions.
(4) The present numerical model yields reasonable predictions of the diameters of most, but not all, of the flames considered. Ignition conditions introduce uncertainties in the experimental and numerical work, indicating a limitation of the 2 s drop tower for these experiments.
(5) The 10 flames have similar profiles of H radical mole fraction in C/O space, with H diminishing near $C/O = 0.53$. H radical reduces soot inception via the propargyl pathway.

Acknowledgments

This work was supported by NASA. The authors appreciate helpful discussions with D.L. Urban and D.P. Stocker and guidance on kinetics from A. Lifshitz.

References

[1] F. Takahashi, I. Glassman, Combust. Sci. Technol. 37 (1984) 1–19.
[2] D.G. Keil, R.J. Gill, D.B. Olson, H.F. Calcote, Proc. Combust. Inst. 20 (1985) 1129–1137.
[3] B.S. Haynes, H.G. Wagner, Prog. Energy Combust. Sci. 7 (1981) 229–273.
[4] M.M. Harris, G.B. King, N.M. Laurendeau, Combust. Flame 64 (1986) 99–112.
[5] I. Glassman, Proc. Combust. Inst. 22 (1988) 295–311.
[6] P. Markatou, H. Wang, M. Frenklach, Combust. Flame 93 (1993) 467–482.
[7] I. Glassman, F.L. Dryer, R.F. Sawyer, Physical and Chemical Aspects of Combustion: A Tribute to Irvin Glassman, Taylor and Francis, 1997.
[8] J. Du, R.L. Axelbaum, Combust. Flame 100 (1995) 367–375.
[9] P.B. Sunderland, D.L. Urban, D.P. Stocker, B.H. Chao, R.L. Axelbaum, Combust. Sci. Technol. 176 (2004) 2143–2164.
[10] B.M. Kumfer, S.A. Skeen, R. Chen, R.L. Axelbaum, Combust. Flame 147 (2006) 233–242.
[11] B.M. Kumfer, S.A. Skeen, R.L. Axelbaum, Combust. Flame 154 (2008) 546–556.
[12] S.A. Skeen, Oxygen-Enhanced Combustion: Theory and Applications, PhD thesis, Washington University in St-Louis, St-Louis, USA, 2009.
[13] R.J. Santoro, T.T. Yeh, J.J. Horvath, H.G. Semerjian, Combust. Sci. Technol. 53 (1987) 89–115.
[14] P.B. Sunderland, G.M. Faeth, Combust. Flame 105 (1996) 132–146.
[15] I. Glassman, Proc. Combust. Inst. 27 (1998) 1589–1596.
[16] R.A. Dobbins, Combust. Flame 130 (2002) 204–214.
[17] R.A. Tesner, S.V. Shurupov, Combust. Sci. Technol. 92 (1993) 61–67.
[18] D.X. Du, R.L. Axelbaum, C.K. Law, Proc. Combust. Inst. 22 (1988) 387–394.
[19] D.X. Du, R.L. Axelbaum, C.K. Law, Proc. Combust. Inst. 23 (1990) 1501–1507.
[20] K.C. Lin, G.M. Faeth, J. Propuls. Power 12 (1996) 691–698.
[21] K.J. Santa, B.H. Chao, P.B. Sunderland, D.L. Urban, D.P. Stocker, R.L. Axelbaum, Combust. Flame 151 (2007) 665–675.
[22] P.B. Sunderland, R.L. Axelbaum, D.L. Urban, B.H. Chao, S. Liu, Combust. Flame 132 (2003) 25–33.
[23] S. Gordon, B.J. McBride, Computer Program for Calculation of Complex Chemical Equilibrium Compositions and Applications, National Aeronautics and Space Administration, Office of Management, Scientific and Technical Information Program, 1996.
[24] R.J. Kee, J.F. Grcar, M.D. Smooke, J.A. Miller, E. Meeks, Premix: A FORTRAN Program for Modeling Steady Laminar One-Dimensional Premixed Flames, Report No. SAND85-8240, Sandia National Laboratories, 1987.
[25] K.J. Santa, Z. Sun, B.H. Chao, P.B. Sunderland, R.L. Axelbaum, D.L. Urban, D.P. Stocker, Combust. Theory Model. 11 (2007) 639–652.
[26] S. Tse, D. Zhu, C. Sung, Y. Ju, C. Law, Combust. Flame 125 (2001) 1265–1278.
[27] R.J. Kee, F.M. Rupley, E. Meeks, J.A. Miller, Chemkin-III: A Fortran Chemical Kinetics Package for the Analysis of Gas-phase Chemical and Plasma Kinetics, Report No. SAND96-8216, Sandia National Laboratories, 1996.
[28] R.J. Kee, G. Dixon-Lewis, J. Warnatz, M.E. Coltrin, J.A. Miller, H.K. Moffat, A Fortran Computer Code Package for the Evaluation of Gas-Phase Multicomponent Transport Properties, Report No. SAND86-8246, Sandia National Laboratories, 1988.
[29] J.F. Grcar, The Twopnt Program for Boundary Value Problems, Report No. SAND91-8230, Sandia National Laboratories, 1991.
[30] B.G. Carlson, K.D. Lathrop, in: H. Greenspan, C. Kelber, D. Okrent (Eds.), Computing Methods in Reactor Physics, Gordon and Breach, New York, 1968, pp. 165–266.
[31] P. Riviere, D. Scutaru, A. Soufiani, J. Taine, Proceedings of the 10th International Heat Transfer Conference, Taylor & Francis, 1994.
[32] L.S. Rothman, A. Barbe, D.C. Benner, L.R. Brown, C. Camy-Peyret, M.R. Carleer, K. Chance, C. Clerbaux, V. Dana, V.M. Devi, J. Quant. Spectrosc. Radiat. Transf. 82 (2003) 5–44.
[33] H. Wang, X. You, A.V. Joshi, S.G. Davis, A. Laskin, F. Egolfopoulos, C.K. Law, USC Mech Version II, High-Temperature Combustion Reaction Model of H2/CO/C1-C4 Compounds, May 2007. <http://ignis.usc.edu/USC_Mech_II.htm>.
[34] S.A. Skeen, G. Yablonsky, R.L. Axelbaum, Combust. Flame 156 (2009) 2145–2152.
[35] S. Tang, M.K. Chernovsky, H.G. Im, A. Atreya, Combust. Flame 157 (2010) 118–126.
[36] S. Tang, M.K. Chernovsky, H.G. Im, A. Atreya, Combust. Flame 157 (2010) 127–136.
[37] R.W. Bilger, Proc. Combust. Inst. 22 (1988) 475–488.
[38] X. Zhou, S. Mahalingam, Combust. Flame 133 (2003) 197–199.